うとやはり矢印 B で示された 30 秒後には A における曲率とほぼ等しい曲率0.02mm^{-1}程度が実現される。なお D-N は先に述べた通り屈曲を示さなかったが、電圧を 5V まで上昇させると屈曲を示し、3V 下での D-S 同様、屈曲緩和も無く、更に高い屈曲制御性を示した。アクチュエータ利用のためには、より低消費エネルギーである事が望ましいので、今後の議論では屈曲に 5V を必要とする D-N には触れない。

C－２．高速振動交流電圧下での屈曲

アクチュエータは長時間高精度の屈曲制御性を示す必要があるので、絶えず電圧値が変動する交流電圧下でその曲率値がどのような振舞いを見せるかを観測した。図 7 は H-N、H-S が印加電圧 V(volt) = 1sin(0.4πt)、V(volt) = 3sin(0.4πt)の交流電界の下、どのような曲率の振舞いを示すかを表したものである。いずれも印加交流電圧に応じて曲率の変化を示すが、曲率の振幅や振動の中心は決して一定には保たれず、アクチュエータ材料として屈曲制御性に問題がある。しかし、図 8 に示す様に D-S は V(volt) = 3sin(0.4πt)の印加電圧のもと、振幅も振動の中心も比較的安定した値を示す。しかもこの性質は最低でも数時間かなりの精度で維持される事が観測された。つまり最低でも数時間という従来に無い長寿命が実現された。なお D-S は V(volt) = 1sin(0.4πt)の下では屈曲を示さない。

D. 考察

イオン交換膜の屈曲を引き起こす為には膜に対する大量の含水が必須と考えられてきたが、むしろ脱水を施す方がその屈曲制御性向上のためには望ましい。また脱水を施す事によって長寿命も実現される。脱水処理によるこの様な性質の向上がなぜ実現されるのかは明らかではないが、含水イオン交換膜に特有の屈曲緩和が観測されない事から、従来とは異なる屈曲メカニズムによるものと考えられる。実際に我々の研究から、脱水 Selemion の屈曲は Selemion 表面のメッキ銀層の酸化還元が寄与しているであろう事が間接的に示唆されており、その点に関し以下に詳述する。

2. 脱水イオン交換膜の屈曲メカニズム

A. 研究目的

既に述べた通り、従来の概念とは逆にイオン交換膜は含水処理を施さずとも屈曲を示し、その屈曲制御性向上、寿命の延長は著しいものであった。ここではなぜ脱水 Selemion の屈曲が引き起こされるのかを明らかにする。

B. 研究方法

B－１．Selemion 表面銀層の酸化還元

先に述べた D-S と同じタイプの試料を用いる。脱水 Selemion は屈曲する際に必ず、印加電圧正極の方向へ屈曲し、Selemion 正極表面上の銀層は白から黒へ変色する。極性を反転すると黒から白へ戻る。つまり正極表面は黒色となり、負極表面は白色となるのである。白色は銀(Ag)の色であるが、黒色は酸化銀(Ag_2O)の色であると考えられる。Ag_2O は高温下で Ag と O_2 に分解する事が知られているが、この黒い物質も 240°C の高温下では白色に戻る。屈曲の際、この変色は必ず引き起こされ、$4Ag + O_2 = 2Ag_2O$ の酸化還元反応が屈曲に寄与している事が示唆される。実際に酸化還元が引き起こされているかどうかを調べる為に以下に述べる実験を行った。

C. 研究結果

C－１．真空中での屈曲

D-S の屈曲に $4Ag + O_2 = 2Ag_2O$ の酸化還元反応が屈曲に寄与しているかどうかを調べるために、酸素(O_2)がほとんど存在しない真空に近い状態の密閉容器中(気圧～100mHg)で

Selemion に 3V の一定電圧を印加する実験を行った。Selemion 正極表面で白から黒への色変化が観測されたが、それは大気中で電圧を印加した場合に得られる黒色よりも薄い黒色で、しかも曲率も大気中での曲率より明らかに小さかった。これは O_2 が不足している環境にあるためであると考えられる。つまり屈曲が引き起こされる際には O_2 が深く関与していることを示唆する。すなわち、酸化還元が屈曲に関与している事を意味する。

C－２．窒素ガス中での屈曲

しかし、O_2 の不足ではなく、単に周囲の気圧が低い事が屈曲性能を低減させた可能性も考えられる。そこで大気圧とほぼ同じ気圧を持つ窒素ガスのみで満たされた密閉容器中で同様な測定を行った。しかしやはり曲率は小さいままだった。つまりこれも屈曲に酸化還元が寄与している事を示唆する実験結果と解釈される。

C－３．微量の含水の必要性

しかし、これら実験を行う仲で、我々は脱水 Selemion の屈曲には極めて微少量ではあるが水が必要であることを見出した。以下に述べるのは微少量の水の必要性を示唆する実験である。

試料 D-S を十分長期に渡ってデシケータ中に乾燥剤と共に保存する。次に 240°C のアイロンで D-S を十分加熱してより完全な脱水を施す。アイロンによる加熱後直ちに D-S 試料を大気中に定められた時間放置し、その直後に 3V の一定電圧を印加して、その曲率の時間依存性を測定した。図 9 はその結果であるが、大気中への放置時間が長いほど曲率値が上昇していることがわかる。これはアイロンによる脱水処理が Selemion 中の極微量の水までも取り去ってしまい、iD-S(0)の様に殆ど水を含んでいない試料は余り屈曲を示す事は無くなってしまうが、大気中に長時間放置された iD-S(15)は大気中から水分を吸収し、その屈曲性を取り戻したと解釈される。更に、この解釈を確かめる為にアイロンによる加熱処理を施した D-S を異なる相対湿度の環境下に数時間以上放置した後に曲率の時間依存性を調べた。図 10 はその結果である。完全にとは言えないが、相対湿度上昇と共に曲率が上昇する傾向にあることが分かる。これは大気中の微量の水が Selemion の屈曲に寄与している事を示唆する。

C－４．酸化還元と屈曲の相関の再検討

これまでの議論を総括すると D-S が低酸素環境中、低気圧中で屈曲しなかったのはむしろただ単に D-S を取り巻く環境に水が不足していたために過ぎなかったとも考えられる。そこで我々は大気圧と同じ気圧の 100％窒素ガス雰囲気を作り出し、相対湿度を 40％から 90％まで変化させて D-S の屈曲試験を行った。結果は相対湿度が上昇するにつれて屈曲が大きくなるというものであった。この結果は屈曲に対する O_2 の必要性を否定し、水が大きく関わっていることを示唆する実験結果のように考えられるが、たとえこの様な環境下であっても屈曲が引き起こされる時は必ず D-S の正極表面は黒色に変化し、極性を反転させると白色に戻った。つまり屈曲にはやはり $4Ag + O_2 = 2Ag_2O$ の酸化還元反応が関与していることは明らかである。今の場合、屈曲試験は 100％窒素雰囲気中で行ったので O_2 は存在しないように思えるが、おそらく、大気中の水分が印加電圧によって電気分解し、酸素が生成したものと思われる。

D. 考察

ここまでの議論で Selemion 表面の Ag の酸化還元が屈曲に寄与しているであろう事が示唆されたが、具体的にどのようなメカニズムによって屈曲が引き起こされているかはまだ明らかではない。しかし、ここで我々は一つの

可能性を紹介する。

Selemion は高分子である故、その表面には激しい起伏があり、例えば(少し誇張してあるが)図 11 に示す様に、所々銀層が Selemion 内部に深く食い込んでいる。それを端的に表した拡大図が図 11(a)である。起伏の激しい Selemion 表面(この場合下面)に大きく開いた口があり、その内部に 4 つの銀原子が捉えられている。酸化が引き起こされると図 11(b)の様に 4 つの銀原子が O に結合し(Ag_2O が生成し)、結果的に大きく開いた口が狭まる。Selemion 上面では(a)→(b)とは逆の過程(還元)である(b)→(a)が引き起こされ、狭まっていた口が大きく開く。つまり下面での「口の狭まり(gap narrowing)」と上面での「口の広がり(gap widening)」によって結果的に Selemion は下方へ屈曲すると考えられる。

E. 結論

本報告書、前半部の「1.脱水イオン交換膜の印加電圧下における屈曲制御性」と後半部「2.脱水イオン交換膜の屈曲メカニズム」両者に対する結論をここに述べる。

従来の概念と異なり、イオン交換膜は含水するのではなく、脱水する方がその性能の向上に寄与すると考えられる。ただし、100%の完全脱水ではなく、極微量の水分を含ませておく必要はある。

銀メッキされた脱水イオン交換膜の場合、その屈曲は銀メッキ層の酸化還元に支配され、従来の屈曲メカニズムと異なり、銀層の酸化還元によるイオン交換膜表面状態の変化がその屈曲に寄与していると推測される。

なお D-S と同じタイプの試料を用いて(サイズは本報告書に述べたものよりも大きく、～2.5cm×～2.5cm 程度)ポンプを試作し、流量 900μl / min を実現した。

F. 研究発表

論文発表

1. Popovic S, Tamagawa H, Nogata F, Taya M: FIBER AND SHEET PAN GELS FOR THE ACTUATOR USE. Research Reports of the Faculty of Engineering, Gifu University, 54, 53-60, (2004).

2. Tamagawa H, Nogata F: Extension of Colacicco's experiment supporting the adsorption theory. J. Colloid and Interface Sci., 275, 113-122, (2004).

3. Tamagawa H, Nogata F, Yagasaki K: An interpretation on the amphoteric gel hardness variance through the potential and hardness measurement. J. Colloid and Interface Sci., 275, 107-112, (2004).

4. Tamagawa H, Nogata F: Bending response of dehydrated ion exchange polymer membranes to the applied voltage. J. Membrane Sci., 243, 229-234, (2004).

5. Tamagawa H, Nogata F, Popovic S: Roles of Ag redox reaction and water absorption inducing the Selemion bending. accepted in J. Membrane Sci., (2004).

プロシーディング

1. Tamagawa H, Nogata F: Improved controllability of a fully dehydrated Selemion actuator. ICCAS 2004, Bangkok, (2004).

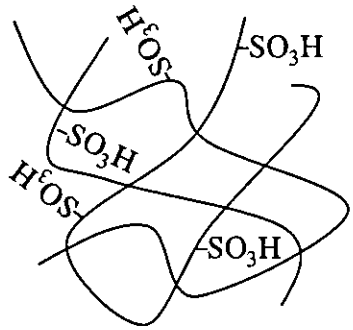

図1　Nafionの分子構造　フルオロカーボン主鎖に$-SO_3H$基がbranchとして存在

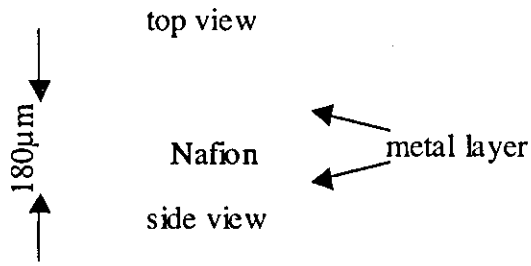

図2　上下面を金属メッキされた梁状Nafion　このNafionは含水状態にあるとする

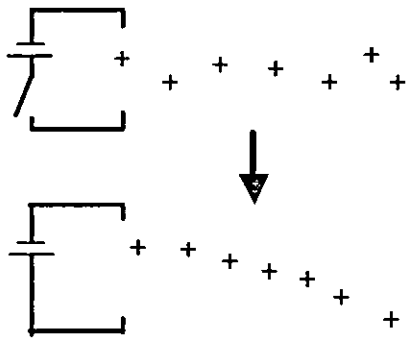

図3　Nafionの屈曲メカニズム　水和カチオンが印加電圧により上方へ引き寄せられ、Nafion 上面から下面へかけて体積勾配が生じ、下方への屈曲が引き起こされる

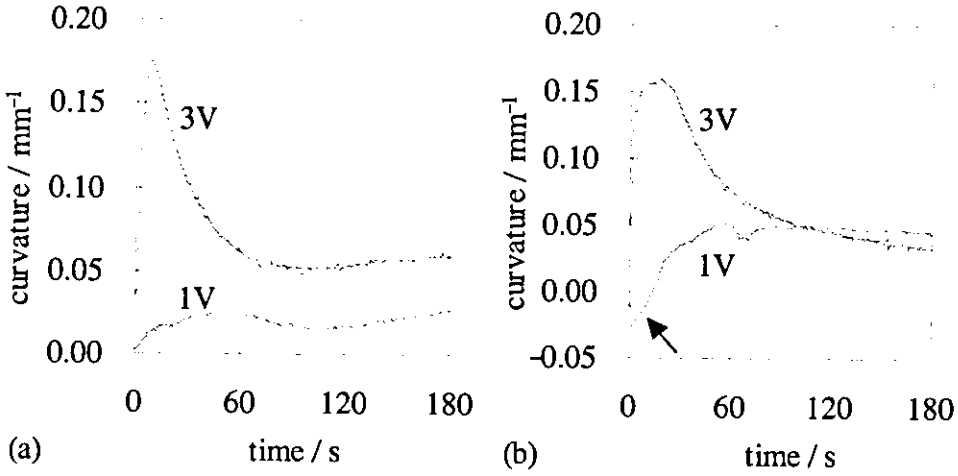

図 4　1V と 3V 下における曲率の時間依存性　(a)H-N　(b)H-S

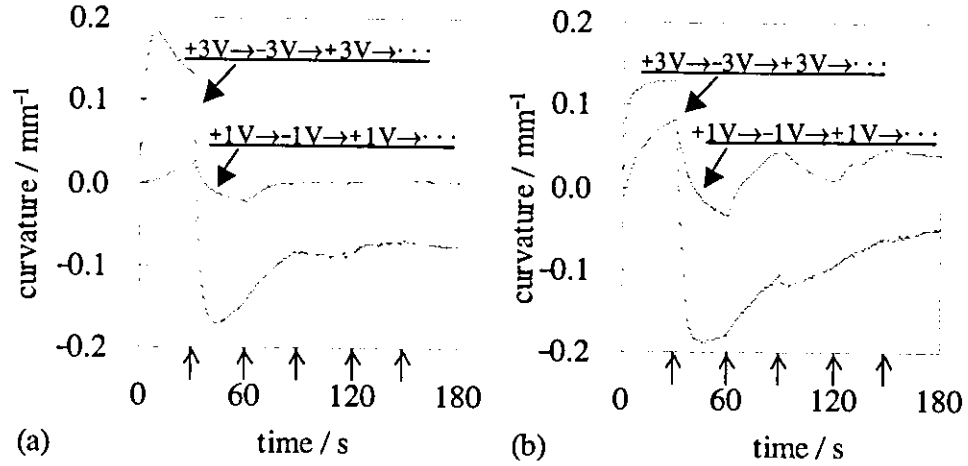

図 4　極性反転を伴う 1V と 3V 印加電圧下における曲率の時間依存性
H-N, H-S いずれも極性反転による+3V→-3V→+3V→・・・、+1V→-1V→+1V→・・・の印加電圧下での曲率変化を示す(a)H-N　(b)H-S

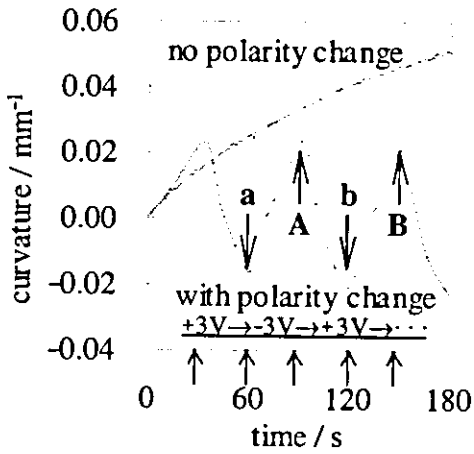

図 5　D-S の 3V 印加電圧における曲率の時間依存性
極性反転がない場合とある場合

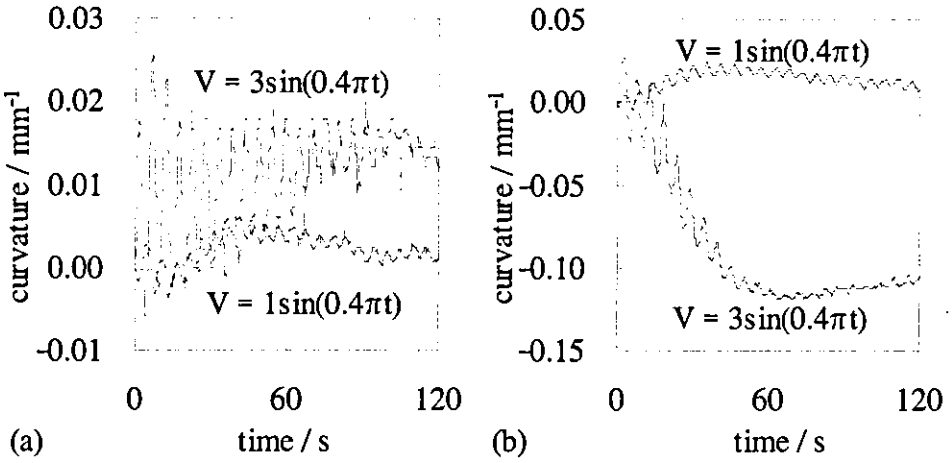

図 7　交流電圧 V(volt) = 1sin(0.4πt)、V(volt) = 3sin(0.4πt)のもとでの曲率の時間依存性　(a)H-N　(b)H-S

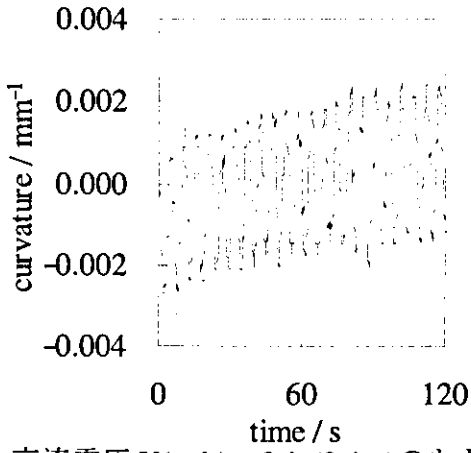

図 8　交流電圧 V(volt) = 3sin(0.4πt)のもとでの D-S の曲率の時間依存性

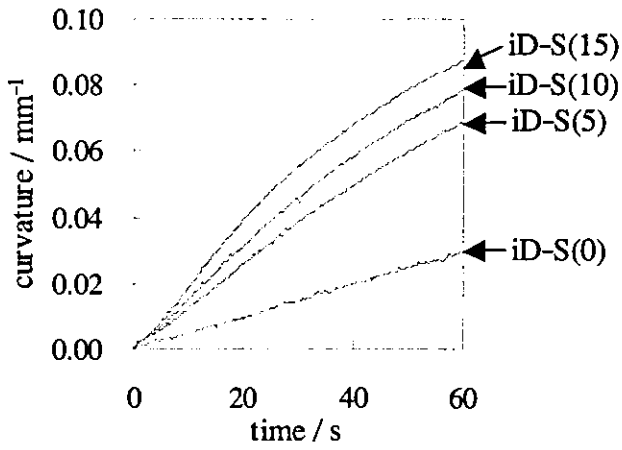

図 9　印加電圧 3V のもとでの D-S の曲率の時間依存性

iD-S(0)、iD-S(5)、iD-S(10)、iD-S(15)はアイロンによる加熱脱水後、大気中にそれぞれ 0、5、10、15 分間放置した試料である事を意味する。

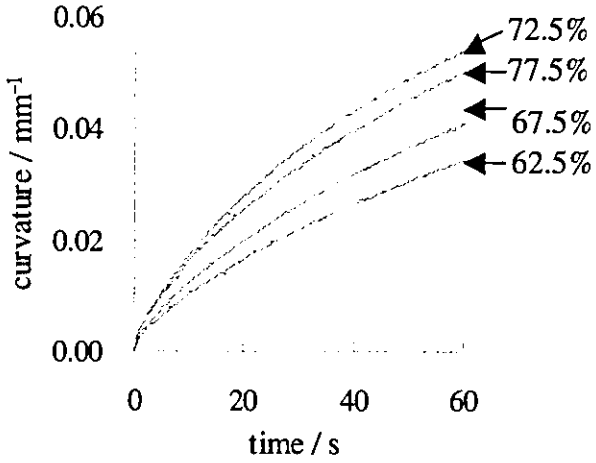

図 10　一定印加電圧のもとでの D-S の曲率の時間依存性
それぞれ相対湿度 62.5、67.5、72、5、77.5％の下で測定した

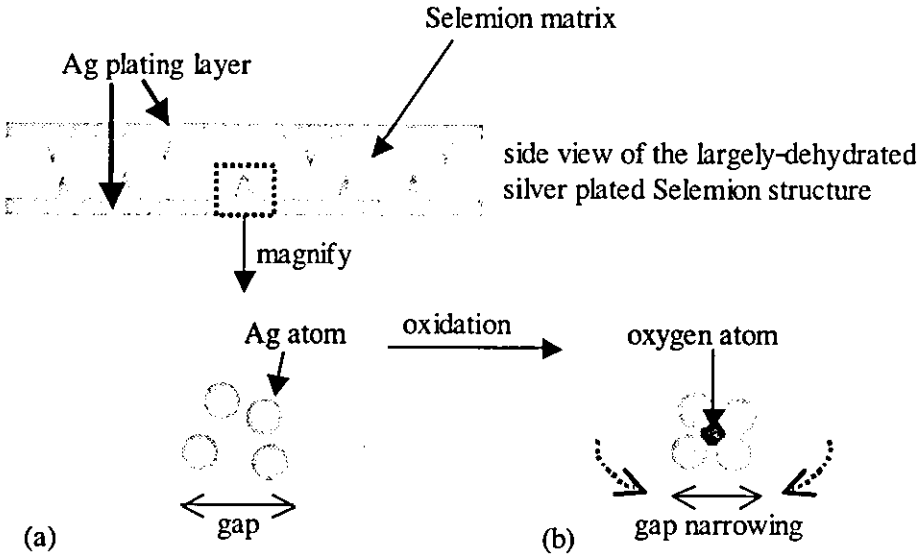

図 11　銀メッキされた脱水 Selemion 構造の側面図　(a)起伏の激しい Selemion 表面(この場合下面)に大きく開いた口があり、その内部に 4 つの銀原子が捉えられている。(b)酸化によって 4 つの銀原子が O に結合し(Ag_2O が生成し)、結果的に大きく開いた口が狭まる。 Selemion 上面では(a)→(b)とは逆の過程(還元)である(b)→(a)が引き起こされ、狭まっていた口が大きく開く　結果的に下方へ屈曲

別紙５

研究成果の刊行に関する一覧表

発表者氏名	論文タイトル	発表雑誌名	巻号	ページ	出版年
Watari,F., Yokoyama, A., Omori,M., Hirai,T., Kondo,H., Uo,M., Kawasaki,T.	Biocompatibility of materials and development to functionally graded implant for bio-medical application.	Composites Science and Technology.	64	139-142	2004
K.Tamura, N.Takashi, T.Akasaka, I.D.Rosca, M.Uo, Y.Totsuka and F.Watari	Effects of micro/nano particle size on cell function and morphology	Key Engineering Materials	254-256	919-922	2004
K.Tani, F.Watari, M.Uo, M.Morita	Fluorescent properties of porcelain-restored teeth and their discrimination	Materials Transaction	45	1010-1014	2004
M.K.Yamada, M.Uo, S.Ohkawa, T.Akasaka and F.Watari	Non-contact surface morphology analysis of CO_2 laser-irradiated teeth by scanning electron microscope and confocal laser scanning microscope	Materials Transaction	45	1033-1039	2004
K.Iwasaki, S.Ohkawa, M.Uo, T.Akasaka and F.Watari	Laser welding of titanium and dental precious alloys	Materials Transaction	45	1040-1146	2004
K.Iwasaki, S.Ohkawa, I.D.Rosca, M.Uo, T.Akasaka and F.Watari	Distortion of laser welded titanium plates	Dental Materials Journal	23	593-599	2004
S.Ohkawa, K.Ishii, M.Uo, T.Sugawara and F.Watari	Slip casting of titanium powder for dental prothetic appliance	Materials Transaction	45	1132-1139	2004
M.K.Yamada, M.Uo, S.Ohkawa, T.Akasaka and F.Watari	Three-dimensional topograhic scanning electron microscopeand raman spectroscopic analyses of the irradiation effect on teeth by Nd:YAG, Er:YAG and CO_2 lasers	Journal of Biomedical Materials Research, Part B: Applied Biomaterials	71	7-15	2004
田中　聡、百理文夫、飯田順一郎	繊維強化プラスチック型審美矯正ワイヤーの湿潤環境下での機械的特性挙動	歯科材料・器械	23	29-39	2004
B.Fugetsu, S.Satoh, T.Shiba, T.Mizutani, Y.Nodasaka, K.Yamazaki, K.Shimizu, M.Shindoh, K.Shibata, N.Nishi, Y.Sato, K.Tohji, F.Watari	Large-Scale Production of Ba^{2+}-Alginate-Coated Vesicles of Carbon Nanofibers for DNA-Interactive Pollutant Elimination	Bulletin of Chemical Society of Japan	77	1945-1950	2004
B. Fugetsu, S. Satoh, T. Shiba, T. Mizutani, Y. -B, Lin, N. Terui, Y. Nodasaka, K. Sasa, K. Shimizu, T. Akasaka, M. Shindoh, K. I. Shibata, A. Yokoyama, M. Mori, K. Tanaka, Y. Sato, K. Tohji, S. Tanaka, N. Nishi, F. Watari	Caged Multiwalled Carbon Nanotubes as the Adsorbents for Affinity-Based Elimination of Ionic Dyes	Environmental Science & Technology	38	6890-6896	2004
Kiyotaka Asakura, Wang-Jae Chun, Kazuyuki Tohji, Yoshinori Sato and Fumio Watari	X-ray Absorption Fine Structure Studies on the Local Structures of Ni Impurities in a Carbon Nanotube	Chemistry Letters	34	382-383	2005
S.Suzuki, Y.Koike, K.Fujiwara, W.J.Chun, M.Nomura and K.Asakura	A possibility of XANAM (X-ray aided non-contact atomic force microscopy)	Chemistry Letters	33	636-637	2004

発表者氏名	論文タイトル	発表雑誌名	巻号	ページ	出版年
H.Yasufuku, Y.Ohminami, T.Tsutsumi, H.Niimi, N.Matsudaira, K.Asakura, M.Kato, Y.Sakai, Y.Kitajima and Y.Iwasawa	Observation of element-specific energy-filtered X-ray photoemission electron microscopy images of Au on Ta using a Wien filter type energyanalyzer	Japanese Journal of Applied Physics	43	7682-7688	2004
M.Uo, F.Watari	Rapid analysis of dental metallic restoratives using X-ray Scanning Analytical Microscope	Dental Materials	20	611-615	2004
M.Uo, M.Tanaka, F.Watari	Quantitative analysis of biological specimens by X-ray scanning analytical microscope	Journal of Biomedical Materials Research, PartB	70B	146-151	2004
M.Uo, M.Okamoto, F.Watari, K.Tani, M.Morita, A.Shintani	Rare earth oxide containing fluorescent glass filler for composite resin	Dental Materials Journal	24	1号掲載予定	2005
A. Kasuya, R. Sivamohan, Y. Barnakov, I. Dmitruk, T. Nirasawa, V. Romanyuk, V. kumar, S. Mamykin, K. Tohji, B. Jeyadevan, K. Shinoda, T. Kudo, O. Terasaki, Z. Liu, R. Belosludov, V. Sundararajan, Y. Kawazoe	Ultra-stable nanoparticles of CdSe revealed from mass spectroscopy	Nature Materials	3	99-102	2004
Y. Sato, B. Jeyadevan, R. Hatakeyama, A. Kasuya, K. Tohji	Electronic properties of radial single-walled carbon nanotubes	Chemical Physics Letters	385	323-328	2004
Y. Akimoto, K. Shinoda, B. Jeyadevan, K. Tohji, K. Kaya, T. Matsumoto, M. Waelchli, Y. Kuroda	Synthesis of water-soluble fullerenes and their characterization	Proceedings of 1st International Workshop on WATER DYNAMICS	1	81-82	2004
R. Justin Joseyphus, C. N. Chinnasamy, B. Jeyadevan, A. Kasuya, K. Shinoda, A. Narayanasamy, K. Tohji	Synthesis of ferrite nanoparticles through aqueous process for biomedical applications	Proceedings of 1st International Workshop on WATER DYNAMICS	1	51-53	2004
大森 守、大久保 昭、大坪 誠、田路和幸、橋田俊之	カーボンナノチューブの固化とハイドロキシアパタイト被覆	2003年度 傾斜機能材料論文集	15	10-15	2004
田村 ·央、高師則行、赤坂 司、ロスカ·イオシフ、宇尾基弘、戸塚靖則、田路和幸、亘理文夫	カーボンナノチューブ、ナノ·マイクロ微粒子に対する生体反応	2003年度 傾斜機能材料論文集	15	22-27	2004
佐藤義倫、秋本結輝、大坪 誠、畠山力三、田路和幸	バイオ用カーボンナノファイバーの開発	2003年度 傾斜機能材料論文集	15	34-39	2004
渥美 崇、B. ジャヤデワン、田路和幸	酸化物磁性ナノ粒子の合成と医療応用の検討	2003年度 傾斜機能材料論文集	15	99-104	2004
赤坂 司、佐藤義倫、田路和幸、亘理文夫	糖鎖によるカーボンナノチューブの表面修飾	2003年度 傾斜機能材料論文集	15	116-121	2004
山本 剛、大坪 誠、佐藤義倫、高橋 亨、大森 守、田路和幸、橋田俊之	単層カーボンナノチューブ焼結体の機械的特性に及ぼす不純物の影響	2003年度 傾斜機能材料論文集	15	157-162	2004

発表者氏名	論文タイトル	発表雑誌名	巻号	ページ	出版年
G. -H. Jeong, N. Satake, T. Kato, T. Hirata, R. Hatakeyama, K.Tohji	Simple methods for site-controlled carbon nanotube growth using radio-frequency plasma-enhanced chemical	Applied Physics A	79	85-87	2004
Y.Sato, Y.Akimoto, B.Jeyadevan, K.Motomiya, R.Hatakeyama, K.Tamura, T.Akasaka, M.Uo, A.Yokoyama, K.Shibata, F.Watari, K.Tohji	Size separation of carbon nanotubes for biomedical application	Proceedings of the International Society for Optical Engineering	5593	13-17	2004
Y.Sato, M.Ohtsubo, B.Jeyadevan, K.Tohji, K.Motomiya, R.Hatakeyama, G.Yamamoto, M.Omori, T.Hashida, K. Tamura, T.Akasaka, M.Uo, A.Yokoyama, F.Watari	Biocompatibility of carbon nanotube disk	Proceedings of the International Society for Optical Engineering	5593	623-627	2004
Y. Sawada, T. Arai, Y. Sato, K. Shinoda, B. Jeyadevan, K. Tohji	Application of multi-walled carbon nanotubes to CdS photocatalytic system	Proceedings of 2nd International Workshop on WATER DYNAMICS	2	293-296	2004
川村　暁、羽田紘一	強磁性微粒子の保持力に与える表面磁気異方性の効果 -計算 vs.実測-	粉体及び粉末冶金	51	703-707	2004
川村　暁、羽田紘一	ナノ微粒子の表面磁気異方性による磁気的硬質化と計算機シミュレーションによる検証	2003年度傾斜機能材料論文集		215-218	2004
M. Omori, A. Okubo, M. Otsubo, T. Hashida and K. Tohji	Consolidation of Multi-Walled Carbon Nanotube and Hydroxyapatite Caoting by the Spark Plasma System	Key Engineering Materials	254-256	395-398	2004
M. Omori, A. Okubo, T. Hashida and K Tohji	Preparation of Multi-Walled Carbon Nanotube Compact by the Spark Plasma System (SPS)	粉体および粉末冶金(J. Jpn. Soc. Powder and Powder Metallurgy)	52	115-119	2005
Takamasa Onoki, Kazuyuki Hosoi and Toshiyuki Hashida	Novel Techniques of Hydroxyapatite Coating on Titanium Utilizing Hydrothermal Hot-pressing	Transactions of the Materials Research Society of Japan	29	2675-2678	2004
Takamasa Onoki, Kazuyuki Hosoi and Toshiyuki Hashida	GD-OES Analysis of the Interface Between Titanium and Hydroxyapatite Ceramics Produced by Hydrothermal Hot-pressing	Transactions of the Materials Research Society of Japan	29	2929-2932	2004
山本剛、佐藤義倫、高橋亨、大森守、田路和幸、橋田俊之	放電プラズマ焼結法により作製した単層カーボンナノチューブバルク固化体の機械的特性	日本機会学会論文集	A702	330-337	2005
横山敦郎，松野浩宜，川崎貴生，水越孝典，石川誠,戸塚靖則，野田坂佳伸，宇尾基弘，亘理文夫，向後隆男.	各種顕微鏡および発光分光分析を用いた摘出インプラント周囲組織中のチタンの分析.	北海道歯誌.	25	330-338	2004
Kondo,H., Yokoyama,A., Omori,M., Ohkubo,A., Hirai,T., Watari,F., Uo,M.,Kawasaki,T.	Fabrication of Titanium Nitride/Apatite Functionally Graded Implants by Spark Plasma Sintering.	Materials Transactions.	145	3156-3162	2004

発表者氏名	論文タイトル	発表雑誌名	巻号	ページ	出版年
Yokoyama,A.,Sato,Y.,Nodasaka, Y.,Yamamoto,S.,Kawasaki,T.,Shin doh,M.,Kohgo,T.,Akasaka,T.,Uo, M.,Tohji,K., Watari,F.	Biologocal behavior of hat-stacked carbon nanofibers in the subcutaneous tissue in rats	Nano Letters	5	157-161	2005
Tamagawa H, Nogata F	Extension of Colacicco's experiment supporting the adsorption theory	J. Colloid and Interface Sci.	275	113-122	2004
Tamagawa H, Nogata F, Yagasaki K	An interpretation on the amphoteric gel hardness variance through the potential and hardness measurement	J. Colloid and Interface Sci	275	107-112	2004
Tamagawa H, Nogata F	Bending response of dehydrated ion exchange polymer membranes to the applied voltage	J. Membrane Sci	243	229-234	2004
渋谷真希子、平沖敏文、木村邦衛、鈴木邦明、福島和昭	リポソーム中に存在するスピンラベル剤のESRスペクトルと全身麻酔薬の影響	北海道歯学雑誌	25	68-76	2004
渋谷真希子、鈴木邦明、平沖敏文、木村邦衛、福島和昭	スピンラベル剤のESRスペクトルに対する全身麻酔薬の影響	北海道歯学雑誌	25	229-237	2004
木村邦衛、平沖敏文、渋谷真希子、鈴木邦明、福島和昭	リポソーム中のスピンラベル剤の周辺環境に及ぼす吸入麻酔薬の影響とその温度依存性	北海道歯学雑誌	25	356-367	2004
木村邦衛、平沖敏文、渋谷真希子、鈴木邦明、福島和昭	リポソーム中のスピンラベル剤の周辺環境に及ぼすホスファチジルコリンの種類と温度の影響	北海道歯学雑誌	25	346-355	2004

IV. 研究成果の刊行物・別刷

Available online at www.sciencedirect.com
SCIENCE DIRECT
ELSEVIER
Composites Science and Technology 64 (2004) 893–908
COMPOSITES SCIENCE AND TECHNOLOGY
www.elsevier.com/locate/compscitech

Biocompatibility of materials and development to functionally graded implant for bio-medical application

Fumio Watari[a,*], Atsuro Yokoyama[a], Mamoru Omori[b], Toshio Hirai[c], Hideomi Kondo[a], Motohiro Uo[a], Takao Kawasaki[a]

[a] *Hokkaido University Graduate School of Dental Medicine, Sapporo 060-8586, Japan*
[b] *Institute for Materials Research, Tohoku University, Sendai 980-8577, Japan*
[c] *Japan Fine Ceramics Center, Mutuno 2-4-1, Atsuta, Nagoya 456-8587, Japan*

Abstract

Functionally graded materials (FGM) were fabricated for bio-medical application, especially for implant application, and the effect of gradient structure was evaluated. The titanium/hydroxyapatite (Ti/HAP) and other FGM implants with the concentration changed gradually in the longitudinal direction of cylindrical shape were fabricated by powder metallurgy to optimize both mechanical properties and biocompatibilities or change bioreactivity in each region. Concentration gradient was formed either by sedimentation in solvent liquid or by packing dry powders into mold, followed by compressing and sintering. Electric furnace heating, high frequency induction heating and spark plasma sintering (SPS) methods were used for sintering. SPS could make the stable Ti/HAP FGM. The Brinell hardness decreased gradually from Ti part to HAP part, which contributes for stress relaxation in the implanted region of bone. Tissue response and osteogenesis in animal implantation tests were evaluated from histological observation by optical microscopy and from elemental mapping by EPMA and XSAM (X-ray scanning analytical microscope). Maturation of bone is more advanced in the HAP rich region. The gradient functions in both mechanical properties and biochemical affinity to osteogenesis contribute to the efficient biocompatibility. These results demonstrated that the tissue reaction occurred gradiently in response to the graded structure of FGM, which implies the possibility to control the tissue response through the gradient function of FGM.

Keywords: A. Metal-matrix composites (NMCs); B. Mechanical properties; Biocompatibility; D. Electron microprobe analysis; E. Sintering

1. Introduction

For implants the materials need to satisfy the all-round properties of biocompatibility, strength and corrosion resistance. Titanium (Ti) is one of the best biocompatible metals and used most widely as implant [1]. Hydroxyapatite (HAP), main component of bone and teeth, has bioactive properties for new bone formation [2–4]. Glass [5–7] ia also one of the materials for biomedical use.

Implant may be classified to "implant" as artificial bone for medical use and "dental implant" as artificial tooth for dental use. The specified properties are slightly different depending on their use. The implants in orthopaedics are used mostly as structurally enforced artificial bone which is inserted inside the corpus. Medical implants lay more weight on strength, toughness, torque in mechanical properties and the specific problem of tribology and abrasion resistance in artificial joint. Dental implant is usually much smaller and used to reconstruct the masticatory function, when tooth root is completely lost or extracted. It is set in the jawbone in the manner to penetrate from the inside to the outside of the bone. The function is, therefore, quite different at the inside of bone, outside and at their boundary. In the inside of jaw bone, bone affinity and stress relaxation are important and in the outside of bone, that is, in oral cavity, the sufficient strength is necessary.

The current dental implants composed of a single material, sometimes with a coating layer, are, however, essentially uniform in composition and structure in the longitudinal direction. The conception of FGM (functionally graded materials) [8–18] may be suitable to apply for implant. In Fig. 1 the expected properties of functionally graded dental implant were shown. The

* Corresponding author. Tel.: +81-11-706-4253; fax: +81-11-706-4251.
E-mail address: watari@den.hokudai.ac.jp (F. Watari).

0266-3538/$ - see front matter © 2003 Elsevier Ltd. All rights reserved.
doi:10.1016/j.compscitech.2003.09.005

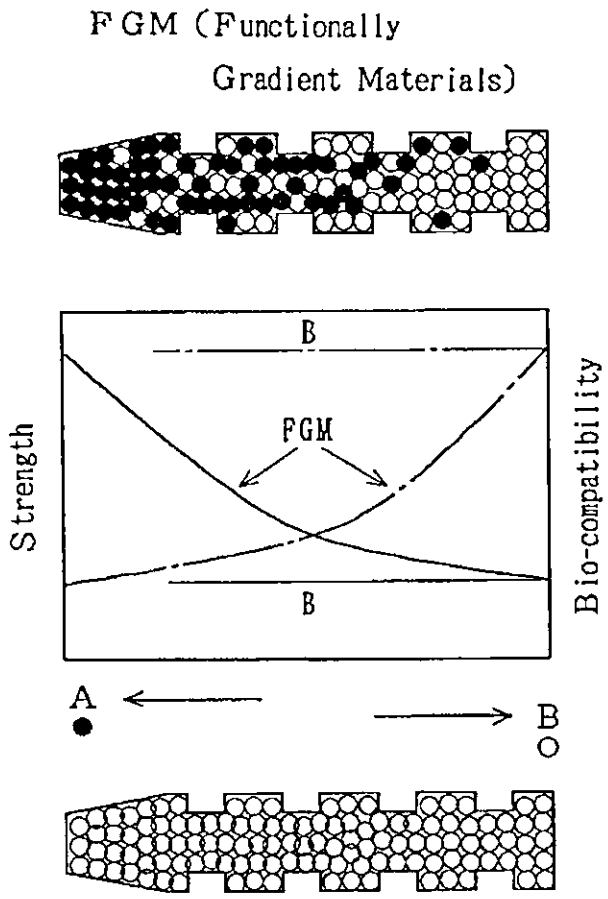

Fig. 1. Expected properties of functionally graded dental implant.

upper schema shows FGM implant and the lower shows the conventional uniform implant. The properties are shown in the middle. For the case of uniform implant the properties such as strength and biocompatibility are constant throughout the implant material. Meanwhile, the implant with the composition changed from the biocompatible metal, Ti, at one end (left in the figure), increasing the concentration of ceramics, HAP, toward 100% HAP at the other end (right), could control the functions of mechanical properties and biocompatibility, depending on the necessity of each part of implant, without the abrupt change due to the formation of discrete boundary. The implant was designed to provide more titanium for the upper part where occlusal force is directly applied and more apatite for the lower part which is implanted inside the jaw bone.

In the followings FGM implant with the structure changed, for example, from pure Ti at one end to Ti–20%HAP at the other end is expressed as Ti/20HAP and the specific region with the composition Ti–20%HAP [19] inside FGM is expressed as Ti-20HAP. Ti/HAP means Ti/100HAP and sometimes the general term for FGM composed of Ti and HAP.

The function of implant may develop further in future to control various bioresponse for the use as a small artificial internal organ. The biomaterials with the conception of FGM structure would serve most properly for this purpose. In the present study the animal implantation tests into both soft tissue and hard tissue were done to investigate the tissue reaction to the gradient composition of FGM structure.

The FGMs of Ti/20HAP [10–12], Ti/100HAP [16–18] and Ti/100Co [14,15] were fabricated by powder metallugy, using the different sintering methods. Ti/ZrO_2, Ti/SiO_2 [9,10], Ti (N)/HAP using surface-nitrided Ti which is expressed as Ti (N), and TiN/HAP were also made and investigated. The other pure metal implants of Ti, Zr, Hf, V, Nb, Ta, Re [1], Ni, Fe, Cu [20–22], Ag and alloys of Ni–Ti, SUS304, SUS316 [22], 12%Au–Ag–Pd–Cu dental alloys were also used for animal experiments for comparison. Laser welded biimplants, composed of combined equal length of metal cylinders, were also investigated in the system of Ti|Zr, Ti|Hf, T:|▽.

Another type of application, the polymer-ceramics FGM, was also done for dental core and post which is used for the case where most of tooth crown is lost and root is still remained [23,24]. Post is inserted in root canal after endodontic treatment and a crown made of metal or other materials is set on the core part to restore the mastication function. Photo-polymerization type composite resin with ceramics filler in polymer resin matrix was used as material. Functionally graded core and post was fabricated by laser lithography, one of the photo-curing type CAD/CAM systems, for stress relaxation at the tooth root by decreasing the filler content ratio from core part down to the apex of post.

In the present paper we focus the main attention on Ti/HAP FGM implant since this is the most interesting and promising for clinical application. This system is, however, not easy to fabricate since the optimum conditions of sintering for Ti and HAP is very different and the sintering condition for their mixture is obliged to make compromise. In the following some of the accomplishments are shown on fabrication, imaging as evaluation, mechanical properties, animal implantation tests and their problems of FGM as well as uniform metals, alloys and biimplants,

2. Experimental procedure

2.1. Implant materials

Table 1 summarizes the specimen preparation methods for uniform, biimplant and gradient implant specimens used in this study. FGM implants were prepared by powder metallurgy, changing gradually the concentration along the longitudinal direction either by dry method or wet method. In the dry method the mixed powders with the varying concentration of 99.98% Ti or Ti hydrate (Sumitomo Sitix) and HAP (Sumitomo Osaka Cement)

Table 1
Specimen preparation methods for uniform, biimplant and gradient implant specimens

Gradient Formation
Dry: Powder packing Wet: Sedimentation
Condensation + Sintering
CIP (Cold Isostatic Press: 400–1000 MPa) + EF (Electric Furnace heating: 1300 °C)
CIP (400 MPa) + HF (High Frequency Induction Heating: 1200 °C)
SPS (Spark plasma sintering: 20–80 MPa, 850 °C) LW (Laser Welding: Nd–YAG, pulse mode, for biimplant).

or 99% Co were packed into the mold. In the wet method [14], two kinds of Ti powders (<45 μm and <150 μm) and two kinds of HAP powders (<20 μm and 20–45 μm) were mixed and stirred in methanol. After the mixture was poured into the tube of 4 mm in an inner diameter and left for sedimentation, the supernatant was removed and dried at 40 °C.

Electric furnace heating [10–15], high frequency induction heating [9–12] and spark plasma sintering (SPS) methods [16–19] were used for sintering. In the electric furnace heating, powders were packed into the thermo-contractive tube with a 0.25 mm thickness. After the heat treatment of a tube at 60 °C, Ti/20HAP and Ti/Co were compressed by CIP (Cold Isostatic Press) at 800–1000 MPa. The implants of the miniature cylindrical shape 2×7 mm or 3×7 mm were then made by sintering in vacuum of 10^{-3} Pa at about 1300 °C for pure Ti, Ti/20HAP, Ti/100HAP FGMs and at 1100 °C for Ti/Co FGM.

In the high frequency induction heating, powders were packed into the thermo-contractive tube or silicone rubber impression mold with the shape of dental implant. After CIP the compacts were sintered at above 1300 °C in Ar gas atmosphere. Ti/20ZrO_2, Ti/20SiO_2 were also prepared.

For SPS (IZUMITECH) the mixed powders of Ti hydrate (SUMITOMO SITIX) and HAP were packed in graphite mold of 200×(7–14) mm with the gradient composition ranged from pure Ti to 100%HAP in the height direction and sintered at 850 °C under the pressure of 40 or 80 MPa. After sintering, the square rods of 1×1×(7–10) mm, 3×3×7 mm and 2×2×14 mm were cut out for animal implantation test, compression test and three point flexural test, respectively, and mechanically polished up to #2000 on the surface. The various FGM specimens were also prepared: Ti/50HAP, 20HAP/50HAP, 50HAP/80HAP, 20HAP/80HAP, 50HAP/100HAP, Ti (N)/HAP and TiN/HAP.

The uniform implants and biimplants were also prepared for comparison in animal experiments. For pure metal implant the wire of 10×10 mm of 99.9%Ti was used other than Ti rod prepared by powder metallurgy. The wire of 10×7 mm was used for 97%Hf, 99.9%Nb, 99.95%Ta, 99.97%Re and the square rod of 0.5×2×10 mm was used for 99.7%Ni. The alloys of Ni–Ti, SUS304, SUS316, 12%Au–Ag–Pd–Cu dental alloys were also used. Bi-implants were prepared by welding the equal length of metal cylinders for the system of Ti|Zr, Ti|Hf, Ti|V using the dental laser welder (TANAKA LaborLaser TLL7000PLUS).

2.2. Mechanical tests

Specimens prepared and evaluation methods used in this study are listed up in Tables 2 and 3, respectively. Brinell hardness was measured in each region inside the Ti/HAP FGM. Compression test was done with the specimens of 3×3×7 mm and the three point flexural test in gauge length 14 mm [6,7] was done with the specimens of 2×2×14 mm, using the universal testing machine (Instron 4204).

2.3. Animal implantation test

FGM implants as well as uniform implants and biimplants were inserted into hard tissue, bone marrow of femora of rats or tibia of rabbits, for 1–8 weeks and into subcutaneous soft tissue in the dorsal or ventral thoracic region for 1–2 weeks. Pure Ti was implanted in every case for comparison.

2.4. Observation and analysis

To observe the implant surface and mechanically polished cross section before implantation and to evaluate the tissue response and osteogenesis after implantation, the observation by optical microscopy (Olympus Vanox-S, Zeiss Axioskop 50), scanning electron microscopy (SEM/Hitachi S2380N, S4000), and elemental line analysis, mapping by EPMA (electron probe microanalysis/JEOL JXA8900) and XSAM (X-ray scanning analytical microscope/Horiba XGT2000V) [20–22] were performed. After the tissue blocks were fixed, they were dehydrated, embedded in resin or paraffin, sectioned to the thickness 100 μm in hard tissue and 5 μm in soft tissue, respectively, and stained. These specimens were served for histological observation by optical microscopy. The unstained, thick specimens with only one side polished were used for compositional image by SEM and elemental mapping by EPMA and XSAM. The spatial resolution of mapping is about 1 μm in higher magnification by EPMA and 100 μm by XSAM.

3. Results

Fig. 2 is the SEM image of the cross section of Ti/20HAP FGM implant around the region biased toward

Table 2
Prepared specimens

Materials	Preparation method	Ref.
Pure metals, alloys, composites (uniform composition)		
Ti, Zr, Hf, V, Nb, Ta, Re		[1]
Ti, Ni, Fe, Cu		[20,21]
Ti, Ni, Fe, Cu, TiNi, SUS304, SUS316		[22]
Ag, 12%Au–Ag–Pd–Cu		
Ti–HAP	SPS	[19]
Biimplant		
Ti|V, Ti|Zr, Ti|Hf	LW	
Functionally graded implant		
Ti/20HAP, Ti/Co	CIP + EF	[14,15]
Ti/20SiO_2, Ti/20ZrO_2, Ti/30HAP	CIP + HF	[9,10,12]
Ti/30HAP, Ti/50HAP, Ti/HAP (Ti/100HAP)	SPS	[16,17,18]
50HAP/100HAP, 70HAP/100HAP	SPS	
20HAP/50HAP, 50HAP/80HAP, 20HAP/80HAP	SPS	
TiN/HAP, Ti (N)/HAP	SPS	

Table 3
Evaluation methods for uniform, biimplant and gradient implant specimens

Imaging
Visual
OM (optical microscope)
  Reflection
  Transmission (histopathological observation of implanted tissue)
SEM (scanning electron microscope)
EPMA (electron probe microanalysis)
XSAM (X-ray scanning analytical microscope)

Spectroscopy
WDS (wavelength dispersive spectroscopy)-EPMA
EDS (energy dispersive spectroscopy)-XSAM
Raman spectroscopy

Mechanical test
H.. (Brinell hardness)
σ_c (compressive strength)–compression test
σ_c (flexural strength)-three point flexural test

Biocompatibility test
Implantation in hard tissue and in soft tissue of rat

Ti–20HAP in the right end. The implant has the miniature cylindrical shape of 20×7 mm. The distribution of HAP particles could be recognized inside the Ti matrix. Most of HAP particles are less than 100 μm and their density was increased toward the right.

Fig. 3 shows the Ti (a), P (b) and Ca (c) mapping images by XSAM of Ti/100HAP FGM prepared by sedimentation method. The content of Ti decreases toward the right end and that of Ca, component of HAP, decreases toward the left end. The contrast looks complementary for Ti and Ca. At each end the composition is nearly pure Ti and HAP. However, the changing manner of concentration in P mapping is not the same as that of Ca (Fig. 3b). In the direction from right to left P content was abruptly decreased to nearly null in the center-right, approximately quarter sized region of the whole length and reappeared with lower concentration in the left-half region.

Fig. 4 shows the Ti/HAP FGM after Brinell hardness test observed in profile imaging mode by reflection electrons in SEM. FGM was made by dry method with electric furnace sintering at 1300 °C. The size of round

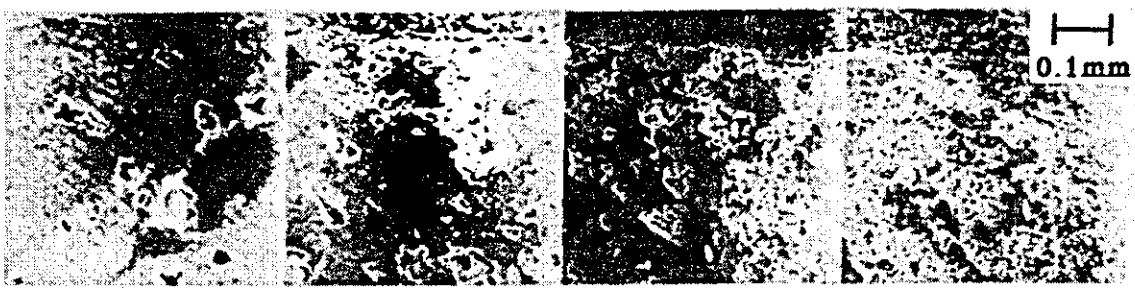

Fig. 2. SEM image of the cross section of Ti/20HAP FGM implant around the region biased toward Ti–20%HAP (right side).

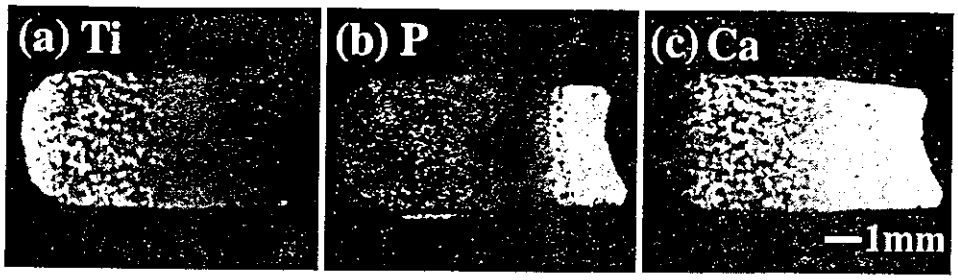

Fig. 3. XSAM elemental mapping of Ti/HAP FGM formed by sedimentation method. a:Ti, b:P, c:Ca.

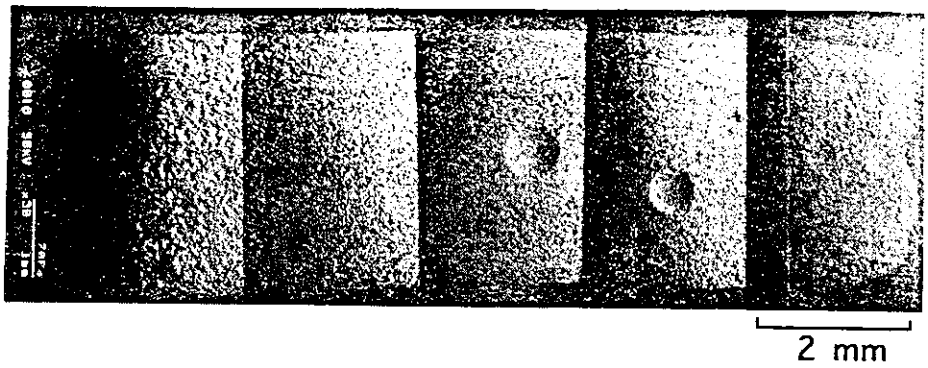

Fig. 4. Ti/HAP FGM after Brinell hardness test observed in profile imaging mode by reflection electrons in SEM where the size of round indentations made by testing in each region indicates the change of hardness.

indentations made by testing expresses the change of hardness from region to region.

Brinell hardness changed with HAP content in the Ti/HAP FGM corresponding to Fig. 4 is shown in Fig. 5a (dotted line). The hardness was about 70 in both Ti and HAP region, and low in the center region where Ti and HAP were mixed with comparable content. There occurred the delayed expansion, followed by spontaneous destruction, after 1 month in this specimen.

Fig. 6 shows the various FGM specimens composed of Ti and HAP, made by SPS method. In the right direction HAP content is increased. Fig. 6a is Ti/50HAP, b is 20HAP/50HAP, c is 50HAP/80HAP, d is 20HAP/80HAP and e is 50HAP/100HAP. Ti/100HAP made by SPS is shown later in Fig. 12a. All these specimens prepared by sintering at 850 °C under 80 MPa using SPS method are stable and endurable to the process of machining, animal implantation and evaluation process.

Fig. 5b (solid line) shows the change of Brinell hardness with HAP content in the Ti/100HAP FGM made by SPS corresponding to Fig. 12a. Ti/HAP FGM is composed of eleven layers with the composition difference by every 10%. Brinell hardness decreased from 61 in pure Ti to 15 in pure HAP, which is the different tendency from Fig. 5a.

The dependence of compression and flexural strength of Ti/HAP FGM on SPS pressure was investigated. For SPS pressure 40 and 80 MPa, compression strength increased increased from 47 to 88 MPa and flexural strength remarkably from 7 to 36 MPa. The fracture in flexural test occurred inside the single layer situated in the center for 80MPa as seen in Fig. 12a. For 40 MPa fracture occurred, deviated from center, in the weaker HAP-rich side and the value (7 MPa) is shown for reference.

Fig. 7 is the external appearance (left) and cross-section (right) of Ti/20HAP FGM dental implant. The upper part, which situates inside the mouth and needs the mechanical properties, is composed of pure Ti, while in the lower part, which situates inside the jaw bone, the content of HAP increases toward the lower up to 20% apatite in the end to provide more biocompatibility.

Fig. 8 shows the subcutaneous soft tissue of rat around Ni after 2 week implantation. Ni implant had been inserted in the hole situated in the center. Observation by optical microscopy (a) and Ca (b), Fe (c), Ni (d) mappings by XSAM were compared. The severe inflammation, hemorrhage and necrosis were induced around Ni implant (Fig. 8a). The inflammatory area observed by optical microscopy (Fig. 8a) corresponds well to the dissolved region of Ni revealed by Ni mapping of XSAM (Fig. 8d). The dissolved concentration of Ni was in the level of 100 ppm [22] and decreased as a function of distance from Ni surface. There was a good relation between the gradient concentration of dissolved Ni and the degree of degeneration of tissue. The region of hemorrhage which looks black in the optical microscopic image (Fig. 8a) corresponds well to the distribution of Fe in Fig. 8c which was contained in hemoglobin. It looks that there was the enrichment of Ca, surrounding Ni implant.

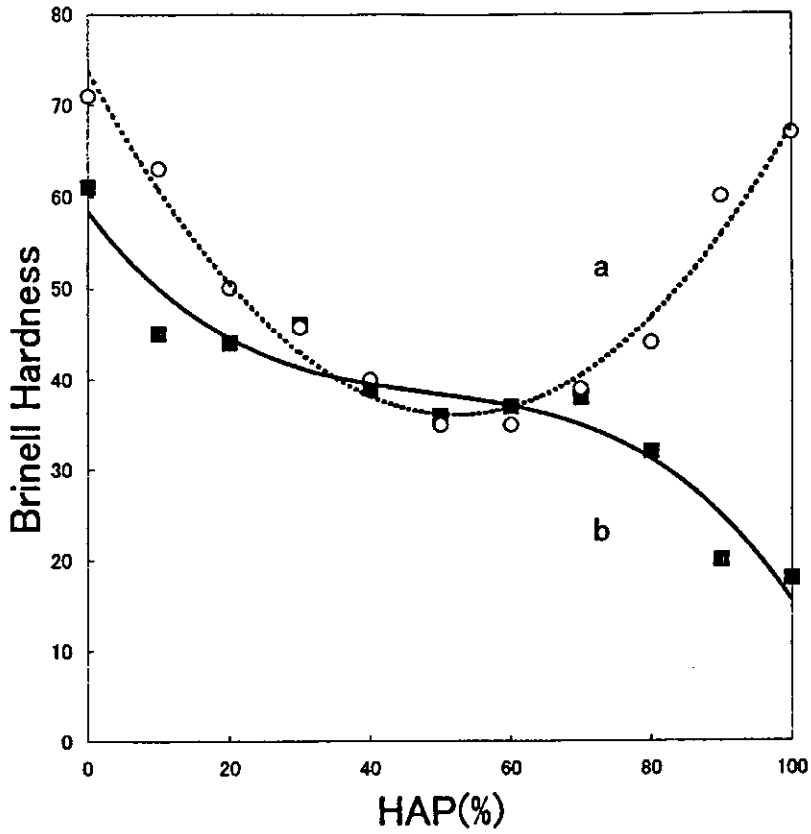

Fig. 5. Change of Brinell hardness with HAP content in Ti/HAP FGM; a is corresponding to FGM of Fig. 4, sintered by electric furnace heating at 1300 °C; b is corresponding to Fig. 12a, sintered by SPS at 850°C.

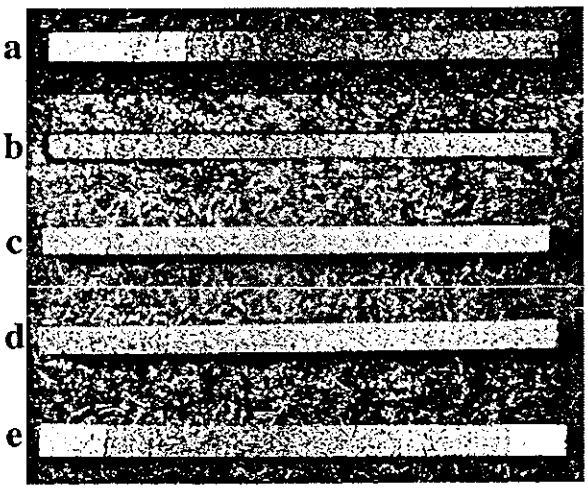

Fig. 6. Various FGM specimens composed of Ti and HAP, made by SPS method (right: HAP rich region): a: Ti/50HAP, b: 20HAP/50HAP, c: 50HAP/80HAP, d: 20HAP/80HAP, e: 50HAP/100HAP.

Fig. 9 shows the comparison of tissue reaction to Ni (a), Ti (b), Fe (c), Ag (d), NiTi (e) and SUS316 (e) after 1 week implantation in the dorsal thoracic region of rat. Implant had been situated in the upper space of each photograph. Fibrous connective tissue was formed around Ti, Fe and Ni–Ti, and under the forming process in Ag and SUS316, while necrosis occurred around Ni. In Ni the expansion of capillary vessels was observed and tissue was in necrosis and in degeneration in the distant region. Ti showed the formation of fibrous connective tissue surrounding implant from the earlier stage and the most sound reaction from histopathological view point. In Fe, tissue had little inflammation and the formation of fibrous connective tissue surrounding implant was observed at this stage. NiTi is similar to Ti. The well stained nuclei of fibroblasts were observed more inside the fibrous connective tissue than Ti, which suggests the slightly longer time would be needed to be in the same condition as pure Ti. In both Ag and SUS316 the formation of fibrous connective tissue was not completed yet and was in the process on the way. The comparison makes noticeable the difference of biocompatibility among these metals sensitively.

Fig. 10 shows the Ti/Co FGM specimen and its effect in the soft tissue after 2 week implantation in the subcutaneous tissue of dorsal part of rat. The left side in Fig. 10a is pure Ti and the right is pure Co. The concentration of Co increases from left to right along the longitudinal direction. Fig. 10c shows the histological observation of the fibrous connective tissue formed around implant. The implant which was removed from

Fig. 7. Ti/20HAP FGM dental implant. External appearance is shown in the left and cross-section in the right.

soft tissue had been situated in the upper side of the photograph Fig. 10c. The thickness of the fibrous connective layer was small in the pure Ti region in the left side and increased toward the right side as the concentration of Co increased along the longitudinal direction of FGM. In the right end the tissue was inflammatory and necrosis occurred in some parts.

The elemental mapping of S, P, Ca, Ti and Co was done for the specimen of Fig. 10 by XSAM. S, Ca and P whose concentration was low enough, of the order of 100ppm in soft tissue, were detected by XSAM and showed the distribution in the whole area of soft tissue. The Ti mapping showed no trace of Ti dissolution. The mapping of Co (Fig. 10b) revealed that the dissolution of Co into the surrounding soft tissue was prominent around the right part of implant. The changing concentration of dissolved Co along the implant toward the right is well coincided with the increase of thickness of tissue layer and the degree of inflammatory response in Fig. 10c.

The wires of Ti, Hf, Nb, Ta, Re implanted in rats showed no inflammatory reaction in soft tissue and in hard tissue. They have enough biocompatibility with a slight difference in new bone formation around implant [1].

Fig. 11 is the histological observation of bone formation and resorption around Ti|V biimplant inserted in the tibia of rabit for 4 weeks. In Ti part (a) new bone was formed directly contact to implant, while cortical bone looked absorbed in the part contacting to V and juvenile immature bone was formed with separation from V (b). Ca mapping by EPMA showed that the density of Ca in new bone around Ti is nearly the same as the cortical bone. On the other hand Ca enrichment was inferior in new bone formed around V. In the Ti|Zr and T|Hf biimplants new bone was formed directly contact to metal surface on both sides of biimplants and Ca enrichment was nearly equivalent to the cortical bone.

Fig. 12a shows the Ti/HAP functionally graded implant (left: Ti, right: HAP) made by SPS under the sintering pressure of 80 MPa after three point flexural test. The 11 layers with the composition difference by every 10% can be recognized. The fracture occurred inside the one layer in the center. Fig. 12b and c are the Ca and Ti mappings by EPMA for Ti/HAP FGM after 8 week insertion in the bone marrow of femora of rat. Ca as representative element of HAP is gradually increased in the longitudinal direction to the right inside the implant. Ca, also as representative element of bone, showed the new bone formed surrounding the implant. Lower-left region is cortical bone. Ti (Fig. 12c), inversely and complementarily to Ca, decreased to the right direction.

Fig. 13 is the histological image around the Ti side (a) and the HAP-rich side (b) in the Ti/HAP FGM implant (I) inserted in the bone marrow (BM) of femora of rat for 16 weeks. New bone (NB) was formed with the thicker but wavy external form, less contact to the implant surface, in the Ti rich region, while with the thin and smooth form, directly contact to the implant in the HAP rich region.

Fig. 14 is the enlargement of new bone formation around the HAP rich region (Ti–80HAP) of Ti/HAP FGM shown in Fig. 13. In Fig. 14 a is HAP matrix, b is Ti particles, c is new bone. Non-transparent Ti particles (b) are dispersed in the semi-transparent HAP matrix (a). Transparent new bone (c) is formed in direct contact on the surface of implant material. New bone

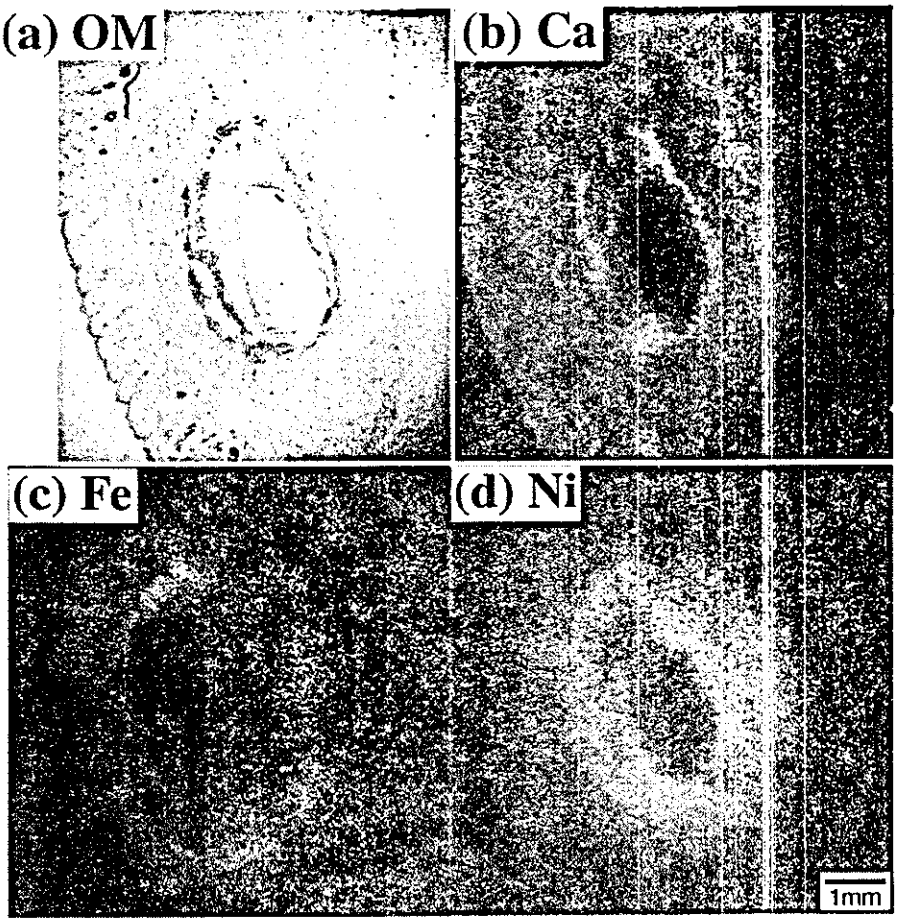

Fig. 8. Subcutaneous soft tissue of rat around Ni after 2 week implantation. Observation by optical microscopy (a) and Ca (b), Fe (c), Ni (d) mappings by XSAM.

showed the lamella structure as a result of bone remodeling, which is the feature of maturation of bone.

4. Discussion

4.1. Fabrication of FGM implant

Ti and HAP is a difficult combination to make FGM by powder metallurgy. The optimum sintering conditions are very different. HAP is stable in the oxidizing atmosphere, while Ti needs the vacuum or reducing atmosphere since Ti is easily oxidized. As sintering temperature HAP needs more than 1150 °C and Ti needs more than 1300 °C. HAP which contains OH^- and 3-PO4 becomes unstable in vacuum and decomposed under the coexistence with Ti particles. Dephosphoration occurs as one of the decomposition phenomena.

XSAM mapping of Ti/HAP FGM prepared by sedimentation method in Fig. 3 showed the gradual decrease of Ca toward the left end. However, the changing manner of concentration in P mapping is not the same as that of Ca (Fig. 3b). Both Ca and P are the main component elements of HAP, therefore both should show the similar concentration gradient. P content was, nevertheless, abruptly decreased to nearly null in approximately one quarter of the whole length to the left direction and reappeared with lower concentration in the center-left region. This suggests the decrease of P content, much lower than that expected from the nominal composition in HAP. Micro-area X-ray diffraction showed the formation of $CaTiO_3$ (Perovskite) in HAP-rich Ti mixed region. In the reducing atmosphere or vacuum at high temperature HAP is unstable when Ti is coexistent and dephosphoration might occur. In this sedimentation method to make the composition gradient, Ti particles sedimented faster at bottom side with its larger density and HAP particles sedimented more slowly due to smaller density. There is also a size distribution in Ti and HAP particles. The larger Ti particles sedimented faster and formed the bottom part, that is, the left end in Fig. 3. The finer Ti particles tended to sediment more slowly and exist more in the supernatant side, that is, HAP rich side in the right. Finer Ti